CHINESE OPTICS LETTERS

Vol. 20, No. 4 | April 2022

Plasmon hybridization induced by quasi bound state in the continuum of graphene metasurfaces oriented for high-accuracy polarization-insensitive two-dimensional sensors

Xiuyu Wang (王秀宇)[1], Jihong Xin (辛继红)[1], Qun Ren (任 群)[2,3*], Haocheng Cai (蔡昊成)[2], Jiaqi Han (韩家奇)[4**], Chengyi Tian (田诚毅)[5], Pengcheng Zhang (张鹏程)[2], Lijie Jiang (蒋丽洁)[2], Zhihao Lan (兰智豪)[6], Jianwei You (游检卫)[3], and Wei E. I. Sha (沙 威)[7***]

[1] Tianjin Key Laboratory of Imaging and Sensing Microelectronic Technology, School of Microelectronics, Tianjin University, Tianjin 300072, China

[2] School of Electrical and Information Engineering, Tianjin University, Tianjin 300072, China

[3] State Key Laboratory of Millimeter Waves, School of Information Science and Engineering, Southeast University, Nanjing 210096, China

[4] Key Laboratory of High Speed Circuit Design and EMC of Ministry of Education, School of Electronic Engineering, Xidian University, Xi'an 710071, China

[5] Huawei Technologies Company Ltd., Shanghai 518129, China

[6] Department of Electronic and Electrical Engineering, University College London, London WC1E7JE, UK

[7] Key Laboratory of Micro-Nano Electronic Devices and Smart Systems of Zhejiang Province, College of Information Science and Electronic Engineering, Zhejiang University, Hangzhou 310027, China

*Corresponding author: renqun@tju.edu.cn

**Corresponding author: jqhan@xidian.edu.cn

***Corresponding author: weisha@zju.edu.cn

Received December 13, 2021 | Accepted February 17, 2022 | Posted Online March 10, 2022

Plasmonics could provide compact and powerful solutions for manipulating light in deep-subwavelength dimensions, which is promising for a great range of nanophotonic technologies such as plasmonic rulers and sensors. However, the effective area of enhanced localized field induced by surface plasmon polaritons is typically restricted to the structural boundaries. In this work, we propose a method to generate high quality-factor extended electromagnetic fields via hybridizing the superradiant state and the quasi bound state in the continuum of graphene metasurfaces. The coupling interaction involved operates as a three-level system with multiple sharp resonances immune to the polarization, which holds great promise for developing nanodevices with high sensing capacity in two dimensions.

Keywords: plasmon hybridization; quasi bound state in the continuum; high-*Q* sensing.

DOI: 10.3788/COL202220.042201

1. Introduction

Localized surface plasmons[1–3], ranging from metals to carbon nanoparticles[4], are among the most powerful and popular label-free measuring[5–7] and sensing techniques[8–10] nowadays due to the interesting physics and important applications such as resonance energy transfer[11,12], field enhancement, and optical tuning capacity[13]. Incorporating plasmonics with metamaterials[14–16] could produce not only electric moment, but also magnetic configuration that achieves effective electromagnetically induced transparency (EIT)-like [17–19] light properties at nanoscale dimensions. However, the lifetime of metallic plasmons is relatively short (tens of optical cycles), which could limit the control of light in fixed nanostructures. Compared with noble-metal plasmonic metamaterials[20–22], plasmons in doped graphene[23–26] are predicted to break the limitation with longer lifespan. Furthermore, due to its unique characteristics of ultrahigh electron mobility and tunable carrier density, the electrical conductivity of graphene can be dynamically tuned by means of chemical, electrostatic, or optical approach.

With the above appealing physical properties, graphene plasmons are promising to construct future compact sensing devices[27–29]. Particularly, the interaction of two or more graphene plasmons causes hybridization between resonance modes,

which could be strong enough to produce dramatic modifications[30–32] in the plasmon field profiles and fine adjustment in the frequency responses. If a plasmon mode is super-radiant, the scattering cross section usually is large and the quality (Q)-factor is low due to the radiation coupling with free space. On the other hand, the subradiant mode typically exhibits larger Q via destructive interference of different radiation channels, which is recently proposed as the bound state in the continuum (BIC)[33,34]. By properly tailoring nanostructures[35–37], BIC could be turned into quasi BIC by introducing symmetry-breaking perturbations. Quasi BIC provides resonant states with ultra-long lifetime in the eigenvalue continuum, which further makes the graphene plasmons live longer. A typical approach to excite high-Q plasmon resonance[38] is achieved via the coupling between quadrupolar and dipolar modes, which involves more energy levels yet limited resonances. Since most spectrum performance in experiments exhibits indistinct resonance lines and spectral shift, more peaks are desired in a few-level system for higher sensing accuracy.

To overcome the limitations mentioned above, in this work, a three-level plasmonic system made of four rotationally aligned graphene strips is proposed for high-resolution and multi-line[39–41] plasmon spectroscopy[42]. We present the intriguing underlying physics of the meta-atom that generates the super-radiant state and the quasi BIC. The equivalent system of linearly coupled Lorentzian oscillators[43–45] is quantitatively described. Here, different from the typical 'dark-bright' arrangement of plasmons, a broken symmetry to the dark mode is introduced for extra channels that determine the measured variables such as nanoscale distance. Additionally, the plasmon hybridization between the quasi BIC and the super-radiant state enlarges the effective area of the localized field by mixing the discrete plasmonic resonance modes, which provide an effective path to sense physical quantities in two dimensions with high accuracy.

2. Structure and Design

The aim of our design is to produce a polarization-insensitive multi-line spectrum with extensive localized field area. Figure 1(a) describes the graphene metasurface fabricated on a quartz substrate, and the unit cell is composed of four rotationally arranged graphene strips, where the periods of the unit cell along the x and y axes are $P_x = P_y = 900$ nm. The resonance mode can be modified via doping and gating since the electron density in graphene strongly depends on the Fermi energy, which will be discussed in the later section. With the chemical potential of 0.6 eV and the relaxation time of 0.33 ps, the absorption spectra of the graphene metasurface with different spacings are investigated, as described in Figs. 1(b) and 1(c). The shorter distance induces more resonance peaks because the discrete plasmons are coupled to one another as the distance between graphene strips decreases. According to the above simulation results, it is easy to find that different distances correspond to different response spectra. When the distance between graphene strips changes in the x or y direction, there is also a distinctive absorption spectrum corresponding to it. Therefore, the graphene metasurface we designed has great application potential in two-dimensional sensing.

To explore the plasmon hybridization effect, finite difference time domain (FDTD)[46] simulation is performed with an incident electromagnetic pulse along the x axis in the frequency range from 30 THz to 45 THz. In addition to the multiple resonances, plasmonic hybridization also contributes to the enlargement of the effective area of enhanced localized field. At the discrete plasmonic mode when the spacing is as large as 150 nm [Fig. 2(a)], the electric field distribution is almost fixed at the boundary of the graphene strips due to the weak coupling interaction. In the hybridized case, however, the localized field is significantly enhanced, and the effective area of the localized field extends to two dimensions induced by the coupling between the super-radiant state and the quasi BIC [magnetic dipole (MD) and electric dipole (ED) indicated in Fig. 2(d)]. As presented in Fig. 2(b), when d is reduced to 100 nm, the discrete plasmonic resonance modes are mixed so that the electric field is distributed in the gaps. When $d = 50$ nm [Fig. 2(c)], the enhanced localized field is further expanded beyond the boundaries of graphene strips. In this case, the coupling between super-radiant modes [ED_1 and ED_2 indicated in Fig. 2(d)]

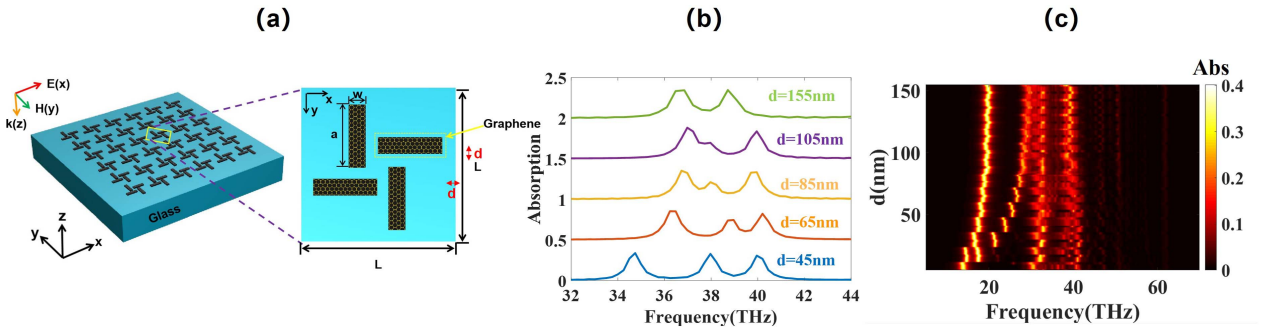

Fig. 1. (a) Schematic view of the proposed graphene metasurface, where the width of graphene strip $w = 300$ nm, length $a = 650$ nm, period $L = 900$ nm, and the polarization is along the x axis. (b) Dispersion map of absorption with different spacings d offset by unity for clarity. (c) Simulated absorption spectra as a function of separation d between graphene strips and frequency.

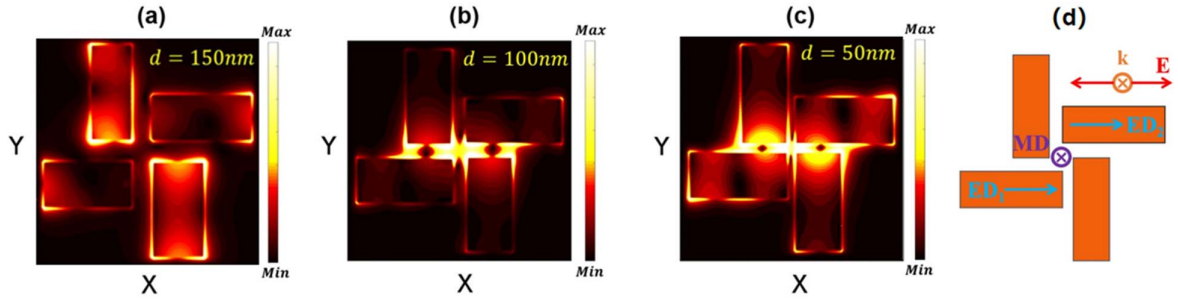

Fig. 2. Localized field distribution 2D plot at 38 THz with different spacings: (a) $d = 150$ nm, (b) $d = 100$ nm, and (c) $d = 50$ nm in the hybridized mode. (d) Indication of the electric dipole (ED) moment and the orthogonal magnetic dipole (MD) moment involved with the super-radiant state and the quasi BIC, respectively.

contributes as well. The hybridization of the ED/MD resonances is typically applied to analyze the optical responses, which will be further discussed in what follows.

3. Results and Discussions

To quantitatively describe the hybridization process of the metasurface, which consists of the artificial states of the super-radiant state $[|1\rangle = \tilde{A}_1(\omega)e^{i\omega t}]$ and the quasi BIC $[|2\rangle = \tilde{A}_2(\omega)e^{i\omega t}]$, a three-level plasmonic system is proposed with the resonance states $|1\rangle$, $|2\rangle$ and the ground state $|0\rangle$. Corresponding resonance frequencies are denoted as ω_{01}, ω_{02}, and the damping factors are δ_1, δ_2 due to the intrinsic dissipation of the system. The super-radiant state induced by the ED moment and the quasi BIC induced by the MD moment hybridize with the external field $(E_0 = \tilde{E}_0 e^{i\omega t})$ having the coupling strength g_1 and g_2, respectively. Defining k as the coupling constant between states $|1\rangle$ and $|2\rangle$, the field amplitude of both states can be represented as linearly coupled Lorentzian oscillators,

$$\begin{pmatrix} \omega - \omega_{01} + \delta_1 & k \\ k & \omega - \omega_{02} + i\delta_2 \end{pmatrix} \begin{pmatrix} \tilde{A}_1 \\ \tilde{A}_2 \end{pmatrix} = -\begin{pmatrix} g_1\tilde{E}_0 \\ g_2\tilde{E}_0 \end{pmatrix}. \quad (1)$$

Solving Eq. (1) above, the amplitudes of super-radiant and quasi BIC resonances are given as

$$\tilde{A}_1 = \frac{[kg_2 - g_1(\omega - \omega_{02} + i\delta_2)]\tilde{E}_0}{(\omega - \omega_{01} + i\delta_1)(\omega - \omega_{02} + i\delta_2) - k^2}, \quad (2)$$

$$\tilde{A}_2 = \frac{[g_2(\omega - \omega_{01} + i\delta_1) - kg_1]\tilde{E}_0}{k^2 - (\omega - \omega_{01} + i\delta_1)(\omega - \omega_{02} + i\delta_2)}. \quad (3)$$

The amplitudes of both states exhibit EIT performance. In the analogue of the metastable level of an atom, as described in Fig. 3(b), the dipole-allowed transition process between the super-radiant mode and light is from $|0\rangle$ to $|1\rangle$, the coupling interaction between the quasi BIC by symmetry breaking and the incident light is from $|0\rangle$ to $|2\rangle$, and the hybridization between the bright mode and the dark mode is from $|1\rangle$ to $|2\rangle$. Two destructive interference processes occur between the pathways $|0\rangle - |1\rangle$ and $|0\rangle - |1\rangle - |2\rangle - |1\rangle$, as well as the pathways $|0\rangle - |2\rangle$ and $|0\rangle - |2\rangle - |1\rangle - |2\rangle$. Figure 3(a) presents the band structure and Q value of the inherent BIC for $|2\rangle$. At around 38 THz, the Q value of its resonance frequency reaches the maximum at the Γ point, and the radiation loss is close to zero. In practice, due to in-plane/out-of-plane symmetry breaking, the BIC converts into quasi BIC with radiation losses and sharp resonance. It can be found in the Fig. 4(d) that super-radiant state and the quasi BIC manifest themselves like EIT. For the proposed structure in this work, via breaking the symmetry of the vertically aligned strips, state $|2\rangle$ is also coupled with incident light and introduces an extra channel in the spectrum for higher resolution.

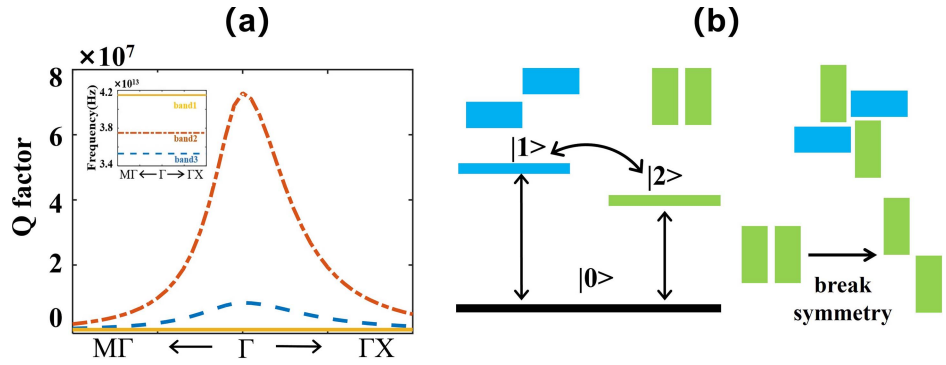

Fig. 3. (a) Q-factor and band structure of BIC mode in the graphene metasurface. (b) Level scheme for the resonances in a schematic three-level system. The super-radiant mode is indicated by blue and the BIC-based mode by green.

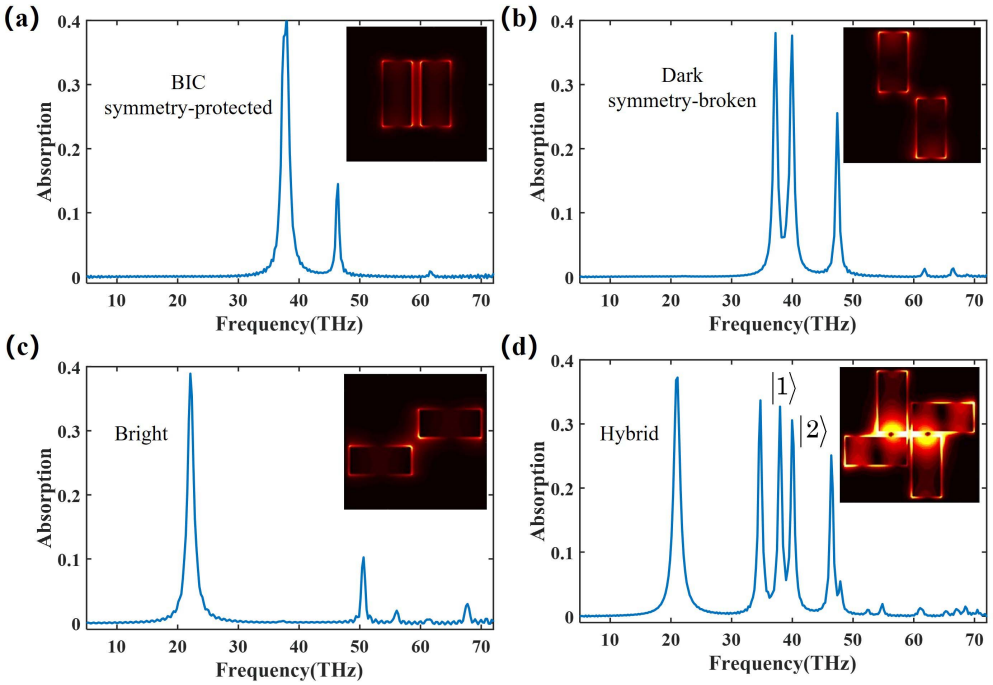

Fig. 4. Absorption spectra and localized field distribution at resonances around 38 THz. (a) Symmetry-protected BIC composed of vertically aligned graphene strips. (b) Quasi BIC via breaking symmetry. (c) Super-radiant (bright) mode composed of horizontal graphene strips. (d) Three-level system for multi-line spectrum via hybridization.

Starting from the symmetric configuration with x-polarized excitation, the optical properties of the graphene metasurface are further explored. Excitation of the quasi BIC can occur when the structural symmetry is broken, giving rise to a high-Q transparency window inside the outer resonance profile and localized field at the boundaries [Fig. 4(b)]. Besides the quasi BIC (state $|2\rangle$), via hybridizing the quasi BIC with bright state located at around 50 THz [Fig. 4(c)], another resonance line appears (state $|1\rangle$) in the spectrum. But, there is some difference between state $|1\rangle$ and the resonance around 50 THz; the former is an excited state, and the latter is the eigenstate. It is clear that the bright state and the quasi BIC are separately coupled with the incident light, and the near field distribution is significantly expanded when the discrete plasmons are coupled. Consequently, owing to the introduction of quasi BIC and the hybridization process with the surface plasmon polarization, more sharp resonances can be generated in this three-level system with an enhanced localized field in two dimensions, which is immune to the polarization.

To further understand the system robustness to the relaxation time induced by the concentration of defective impurities, simulations for the optical spectra are performed based on the FDTD algorithm. As illustrated in Fig. 5(a), when the Fermi energy level is fixed at 0.6 eV, as the relaxation time (τ)

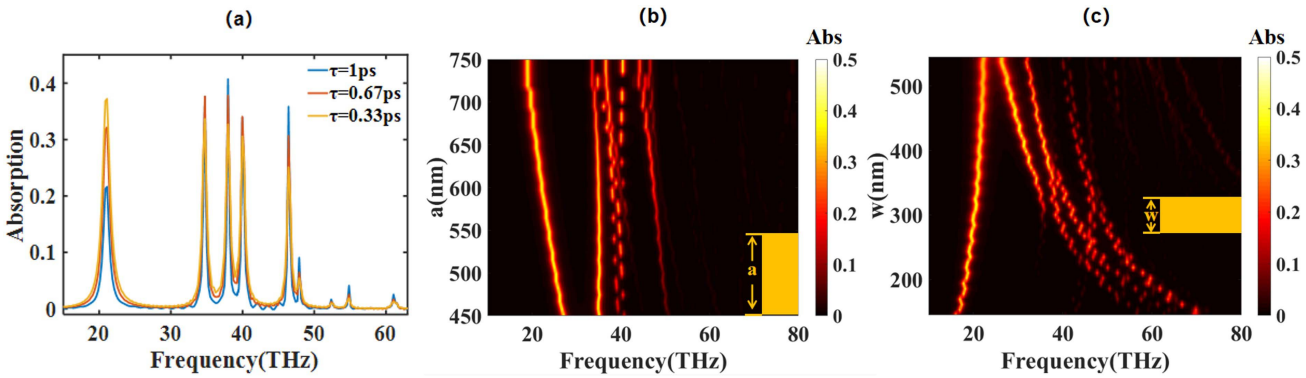

Fig. 5. (a) Absorption spectra versus different relaxation times. (b), (c) Dispersion maps with different lengths and widths of graphene strips. The separation between graphene strips is 45 nm.

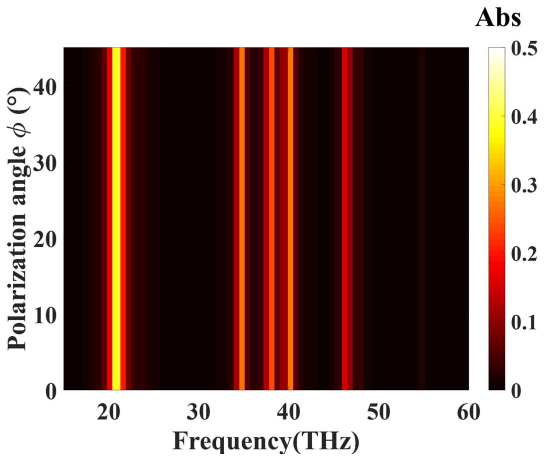

Fig. 6. Simulated absorption spectra as a function of polarization angle ϕ and frequency with 45 nm separation between graphene strips.

decreases, the graphene conductivity decreases, and the electric field becomes weaker. However, the disturbances of relaxation time have little impact on the spectra. This is due to the fact that the BIC-based resonance is exclusively associated with the change of conformation and incident angle. Additional insight into the relationship between the optical resonance and the structural parameter is given in subsequent discussions. When the width of the graphene strip is fixed at 300 nm, as the length increases, the size of the graphene structure gets larger. Consequently, the effective area of the localized field is enhanced accompanied with a strengthened mutual coupling of plamons, and more absorption peaks are generated in the absorption spectra. Similarly, when the length of graphene strips is fixed at 650 nm, as the width increases, the effective area of the localized field gets larger. As such, the coupling between plasmons becomes stronger, and more resonances appear in the spectra. In addition, with the change of length and width, the location of its resonant frequency will also change. As the length increases, the corresponding resonance absorption peak belonging to the bright mode is red-shifted, as shown in Fig. 5(b); as the width increases, its bright mode absorption peak is blue-shifted, and the dark mode absorption peak is red-shifted, as shown in Fig. 5(c). The dependence of the calculated spectral positions of multiple resonances on the structural feature provides high-definition information on the spatial change of the system.

Apart from relaxation time and structural feature, the effect of incident polarization is also investigated. Changing the polarization angle from 0° to 45°, the spectra as plotted in Fig. 6 show that the designed structure is immune to the incident polarization, which is important in practical wide-angle settings.

4. Conclusion

In conclusion, by exploiting the mechanism of plasmon hybridization induced by quasi BIC, a high-Q polarization-insensitive graphene metasurface oriented for sensing in two dimensions is designed. The effective area of the localized electromagnetic field is significantly enlarged via hybridizing different resonance modes, resulting in multi-line spectra in a three-level system, which is immune to the polarization angle of incident light. In addition, the robustness to relaxation time and the effect of structural features on the spectra are also calculated. The proposed graphene-based structure holds great potential for developing compact nanoscale devices with two-dimensional high sensing capacity.

Acknowledgement

This work was partially supported by the National Natural Science Foundation of China (Nos. 12104339, 62174118, 1210040201, U20A20164, and 61975177), Open Fund of State Key Laboratory of Millimeter Wave, Southeast University (No. K202216), International Postdoctoral Exchange Fellowship Program (Talent-Introduction), and China Postdoctoral Science Foundation (Nos. 258023 and 2021M702403).

References

1. J. You, X. Li, F. Xie, W. E. I. Sha, J. H. W. Kwong, G. Li, W. C. H. Choy, and Y. Yang, "Surface plasmon and scattering-enhanced low-bandgap polymer solar cell by a metal grating back electrode," Adv. Energy Mater. **2**, 1203 (2012).
2. S. Sun, H. Chen, W. Zheng, and G. Guo, "Dispersion relation, propagation length and mode conversion of surface plasmon polaritons in silver double-nanowire systems," Opt. Express **21**, 14591 (2013).
3. Y. Zhan, Y. Li, Z. Wu, S. Hu, Z. Li, X. Liu, J. Yu, Y. Huang, G. Jing, H. Lu, H. Guan, W. Qiu, J. Dong, W. Zhu, J. Tang, Y. Luo, J. Zhang, and Z. Chen, "Surface plasmon resonance-based microfiber sensor with enhanced sensitivity by gold nanowires," Opt. Mater. Express **8**, 3927 (2018).
4. Y. Zheng, H. Liu, J. Li, J. Xiang, M. Panmai, Q. Dai, Y. Xu, S. Tie, and S. Lan, "Controllable formation of luminescent carbon quantum dots mediated by the Fano resonances formed in oligomers of gold nanoparticles," Adv. Mater. **31**, 1901371 (2019).
5. M. Olszyna, A. Debrassi, C. Üzüm, and L. Dähne, "Label-free bioanalysis based on low-Q whispering gallery modes: rapid preparation of microsensors by means of layer-by-layer technology," Adv. Funct. Mater. **29**, 1805998 (2019).
6. Y. Kuai, J. Chen, X. Tang, Y. Xiang, F. Lu, C. Kuang, L. Xu, W. Shen, J. Cheng, H. Gui, G. Zou, P. Wang, H. Ming, J. Liu, X. Liu, J. R. Lakowicz, and D. Zhang, "Label-free surface-sensitive photonic microscopy with high spatial resolution using azimuthal rotation illumination," Sci. Adv. **5**, v5335 (2019).
7. F. Wang, B. Chen, B. Yan, Y. Yin, L. Hu, Y. Liang, M. Song, and G. Jiang, "Scattered light imaging enables real-time monitoring of label-free nanoparticles and fluorescent biomolecules in live cells," J. Am. Chem. Soc. **141**, 14043 (2019).
8. N. Liu, M. Mesch, T. Weiss, M. Hentschel, and H. Giessen, "Infrared perfect absorber and its application as plasmonic sensor," Nano Lett. **10**, 2342 (2010).
9. N. Liu, T. Weiss, M. Mesch, L. Langguth, U. Eigenthaler, M. Hirscher, C. Sönnichsen, and H. Giessen, "Planar metamaterial analogue of electromagnetically induced transparency for plasmonic sensing," Nano Lett. **10**, 1103 (2010).
10. H. Tayoub, A. Hocini, and A. Harhouz, "High-sensitive mid-infrared photonic crystal sensor using slotted-waveguide coupled-cavity," Prog. Electromagn. Res. M **105**, 45 (2021).
11. Y. Qin, Y. Fang, L. Wang, S. Tang, S. Sun, Z. Liu, and Y. Mei, "Surface wave resonance and chirality in a tubular cavity with metasurface design," Opt. Commun. **417**, 42 (2018).

12. F. Guan, S. Sun, S. Ma, Z. Fang, B. Zhu, X. Li, Q. He, S. Xiao, and L. Zhou, "Transmission/reflection behaviors of surface plasmons at an interface between two plasmonic systems," J. Condens. Matter Phys. **30**, 114002 (2018).
13. J. Li, Y. Xu, Q. Dai, S. Lan, and S. Tie, "Manipulating light-matter interaction in a gold nanorod assembly by plasmonic coupling," Laser Photonics Rev. **10**, 826 (2016).
14. W. Sun, Q. He, S. Sun, and L. Zhou, "High-efficiency surface plasmon meta-couplers: concept and microwave-regime realizations," Light Sci. Appl. **5**, e16003 (2016).
15. S. Sun, Q. He, J. Hao, S. Xiao, and L. Zhou, "Electromagnetic metasurfaces: physics and applications," Adv. Opt. Photonics **11**, 380 (2019).
16. J. W. You and N. C. Panoiu, "Plasmon-induced nonlinearity enhancement and homogenization of graphene metasurfaces," Opt. Lett. **44**, 3030 (2019).
17. X. Yan, M. Yang, Z. Zhang, L. Liang, D. Wei, M. Wang, M. Zhang, T. Wang, L. Liu, J. Xie, and J. Yao, "The terahertz electromagnetically induced transparency-like metamaterials for sensitive biosensors in the detection of cancer cells," Biosens. Bioelectron. **126**, 485 (2019).
18. C. Wang, X. Jiang, G. Zhao, M. Zhang, C. W. Hsu, B. Peng, A. D. Stone, L. Jiang, and L. Yang, "Electromagnetically induced transparency at a chiral exceptional point," Nat. Phys. **16**, 334 (2020).
19. J. Zhong, X. Xu, and Y. Lin, "Tunable terahertz metamaterial with electromagnetically induced transparency characteristic for sensing application," Nanomaterials **11**, 2175 (2021).
20. N. P. Montoni, S. C. Quillin, C. Cherqui, and D. J. Masiello, "Tunable spectral ordering of magnetic plasmon resonances in noble metal nanoclusters," ACS Photonics **5**, 3272 (2018).
21. A. V. Kabashin, P. Evans, S. Pastkovsky, W. Hendren, G. A. Wurtz, R. Atkinson, R. Pollard, V. A. Podolskiy, and A. V. Zayats, "Plasmonic nanorod metamaterials for biosensing," Nat. Mater. **8**, 867 (2009).
22. C. Gong and M. S. Leite, "Noble metal alloys for plasmonics," ACS Photonics **3**, 507 (2016).
23. D. Z. Manrique, J. W. You, H. Deng, F. Ye, and N. C. Panoiu, "Quantum plasmon engineering with interacting graphene nanoflakes," J. Phys. Chem. C **121**, 27597 (2017).
24. Q. Ren, J. W. You, and N. Panoiu, "Comparison between the linear and nonlinear homogenization of graphene and silicon metasurfaces," IEEE Access **8**, 175753 (2020).
25. Q. Ren, J. W. You, and N. C. Panoiu, "Large enhancement of the effective second-order nonlinearity in graphene metasurfaces," Phys. Rev. B **99**, 205404 (2019).
26. Z. Lan, J. W. You, Q. Ren, W. E. I. Sha, and N. C. Panoiu, "Second-harmonic generation via double topological valley-Hall kink modes in all-dielectric photonic crystals," Phys. Rev. A **103**, L041502 (2021).
27. X. Xiong, Y. Chen, H. Wang, S. Hu, Y. Luo, J. Dong, W. Zhu, W. Qiu, H. Guan, H. Lu, J. Yu, J. Zhang, and Z. Chen, "Plasmonic interface modified with graphene oxide sheets overlayer for sensitivity enhancement," ACS Appl. Mater. Interfaces **10**, 34916 (2018).
28. R. Wang, X. Ren, Z. Yan, L. Jiang, W. E. I. Sha, and G. Shan, "Graphene based functional devices: a short review," Front. Phys. **14**, 13603 (2019).
29. Y. Yin, J. Pang, J. Wang, X. Lu, Q. Hao, E. Saei Ghareh Naz, X. Zhou, L. Ma, and O. G. Schmidt, "Graphene-activated optoplasmonic nanomembrane cavities for photodegradation detection," ACS Appl. Mater. Interfaces **11**, 15891 (2019).
30. Y. Qin, X. Xiong, W. Sha, and L. J. Jiang, "Electrically tunable polarizer based on graphene-loaded plasmonic cross antenna," J. Phys. Condens. Matter **30**, 144007 (2018).
31. Y. P. Chen, W. E. I. Sha, L. Jiang, and J. Hu, "Graphene plasmonics for tuning photon decay rate near metallic split-ring resonator in a multilayered substrate," Opt. Express **23**, 2798 (2015).
32. X. Ren, W. E. I. Sha, and W. C. H. Choy, "Tuning optical responses of metallic dipole nanoantenna using graphene," Opt. Express **21**, 31824 (2013).
33. Q. Ren, F. Feng, X. Yao, Q. Xu, M. Xin, Z. Lan, J. You, X. Xiao, and W. E. I. Sha, "Multiplexing-oriented plasmon-MoS_2 hybrid metasurfaces driven by nonlinear quasi bound states in the continuum," Opt. Express **29**, 5384 (2021).
34. Z. Zhang, F. Qin, Y. Xu, S. Fu, Y. Wang, and Y. Qin, "Negative refraction mediated by bound states in the continuum," Photonics Res. **9**, 1592 (2021).
35. J. Xiang, Y. Xu, J. Chen, and S. Lan, "Tailoring the spatial localization of bound state in the continuum in plasmonic-dielectric hybrid system," Nanophotonics **9**, 133 (2020).
36. Q. Ren, J. W. You, and N. C. Panoiu, "Giant enhancement of the effective Raman susceptibility in metasurfaces made of silicon photonic crystal nanocavities," Opt. Express **26**, 30383 (2018).
37. X. Wang, J. Ma, Q. Ren, M. Wang, Z. Yang, and J. Xin, "Effects of Fe^{3+}-doping and nano-TiO_2/WO_3 decoration on the ultraviolet absorption and gas-sensing properties of $ZnSnO_3$ solid particles," Sens. Actuators B **344**, 130223 (2021).
38. Z. Liu, Y. Xu, Y. Lin, J. Xiang, T. Feng, Q. Cao, J. Li, S. Lan, and J. Liu, "High-Q quasibound states in the continuum for nonlinear metasurfaces," Phys. Rev. Lett. **123**, 253901 (2019).
39. H. Hao, S. Zheng, Y. Tang, and X. Ran, "Design of electromagnetic wave multi-type focusing based on 1-bit metasurface," Prog. Electromagn. Res. M **105**, 79 (2021).
40. Q. Fu, Q. Feng, and H. Chen, "Design and optimization of CPW-fed broadband circularly polarized antenna for multiple communication systems," Prog. Electromagn. Res. M **99**, 65 (2021).
41. X. Lai, Q. Ren, F. Vogelbacher, W. E. I. Sha, X. Hou, X. Yao, Y. Song, and M. Li, "Bioinspired quasi-3D multiplexed anti-counterfeit imaging via self-assembled and nanoimprinted photonic architectures," Adv. Mater. **34**, 2107243 (2021).
42. R. Hao, E. Cassan, Y. Xu, M. Qiu, X. Wei, and E. Li, "Reconfigurable parallel plasmonic transmission lines with nanometer light localization and long propagation distance," IEEE J. Sel. Top. Quantum Electron. **19**, 4601809 (2013).
43. G. Calvaruso and A. Zaeim, "On the symmetries of the Lorentzian oscillator group," Collect. Math. **68**, 51 (2017).
44. J. Applequist, K. R. Sundberg, M. L. Olson, and L. C. Weiss, "A normal mode treatment of optical properties of a classical coupled dipole oscillator system with Lorentzian band shapes," J. Chem. Phys. **70**, 1240 (1979).
45. E. Ott and T. M. Antonsen, "Low dimensional behavior of large systems of globally coupled oscillators," Chaos **18**, 37113 (2008).
46. F. Chen and K. Li, "One-step absolutely stable FDTD methods for electromagnetic simulation," Prog. Electromagn. Res. **100**, 45 (2021).